

On the Flow-Pattern of Shallow Atmospheric Convection

A. van Delden

Institute of Meteorology and Oceanography, University of Utrecht, and Free University of Amsterdam,
De Boelelaan 1085, NL-1081 HV Amsterdam, The Netherlands

(Manuscript received December 1987; revised form February and April 1988)

Abstract

It is shown through numerical simulation that open convection cells can only exist when the greatest static (in the absence of convection) thermal instability is located near the lower boundary of the layer, for instance in conditions when cold air is advected over a relatively warm ocean. On the other hand, closed cells can only exist when the flow is driven mainly from the top, for instance by cloud-top radiative cooling, which, due to the high degree of cloud-cover, is precisely most effective in these conditions.

It is also shown that, in the absence of mean vertical wind-shear, shallow convection has a very low "toroidal degree" (i.e. the vertical component of the vorticity is hardly excited), implying that the flow is almost poloidal. This is interesting because the equations of motion for poloidal flow are very similar to those for two-dimensional flow in which only one component of the vorticity is non-zero. It is speculated that the nonlinear dynamics of poloidal flow (and therefore also of convection) is very similar to the nonlinear dynamics of two-dimensional flow.

Zusammenfassung

Über das Strömungsbild flacher atmosphärischer Konvektion

Es wird durch numerische Simulation gezeigt, daß offene Konvektionszellen nur existieren können, wenn die stärkste thermische Instabilität (ohne Konvektion) nahe der unteren Berandung auftritt, wie beispielsweise, wenn über der relativ warmen See Kaltluft advehiert wird. Andererseits können geschlossene Zellen nur dann auftreten, wenn die Strömung von oben her angetrieben wird, beispielsweise durch Strahlungsabkühlung des Wolkenoberrandes, welche aufgrund eines hohen Bedeckungsgrades dabei den wichtigsten Effekt verursacht.

Es wird zudem gezeigt, daß, wenn keine mittlere Vertikalwindscherung auftritt, flache Konvektion sich nur sehr schwach torisch verhält, d.h. die Vertikalkomponente der Vorticity kaum ausgebildet und die Strömung deshalb wesentlich poloidal ist. Dies ist interessant, weil die Bewegungsgleichungen für eine poloidale Strömung sehr ähnlich denen für eine rein zweidimensionale Strömung mit nur einer nicht verschwindenden Vorticitykomponente sind. Man kommt so auf den Gedanken, daß die nichtlineare Dynamik einer poloidalen Strömung (und damit auch von Konvektion) sich sehr ähnlich zur nichtlinearen Dynamik einer zweidimensionalen Strömung verhält.

1 Preface

This paper is concerned with the flow-pattern associated with mesoscale (horizontal scale: 3 to 100 km) cumulus cloud patterns observed so frequently from satellites.

Because of the obvious similarity between the so-called Rayleigh-Bénard thermal convection patterns, observed in the laboratory in a layer heated from below, and the cloud patterns in the atmosphere, the theory of Rayleigh-Bénard convection is taken as the basis of the theoretical explanation of these cloud-patterns.

Both in the laboratory and in the atmosphere one can distinguish three types of convection-planforms: rolls (clouds organized into parallel strips or bands), cells

with downward flow in the centre (called "open cells" in the atmosphere, because they typically have a low cloud-cover) and cells with upward flow in the centre (called "closed cells" in the atmosphere, because they typically have a high degree of cloud-cover).

The planform is not the only interesting aspect of the flow-pattern. Some attention will also be paid to what will be called the *toroidal degree* of the flow. This is a measure for the relative importance of the vertical component of the vorticity. The numerical simulations described in this paper will show that the toroidal degree may be very low (much less than 1%). This implies that convection is nearly poloidal. It will be shown in another paper that poloidal flow has certain features in common with two-dimensional flow.

2 The Planform of Convection: Introduction

Open and closed cells have in common the fact that the centre cloudy or clear area is greater than the periphery. If it is assumed that clouds are correlated perfectly with upward motion and clear areas are correlated perfectly with downward motion, *then open and closed cells are dynamically equivalent*, except that the definition of what is up and down is reversed. This suggests that a parameter (if there is one) which determines the cell-circulation direction just changes sign when there is a transition from open to closed cells or vice-versa.

This has indeed been suggested by several authors. Krishnamurti (1975a) demonstrated that the sign of the large-scale vertical motion may determine whether open or closed cells occur. She found that open cells occur when there is subsidence, while closed cells occur when there is large scale upward motion. Subsequent observational studies (e.g. Busack et al., 1985) have not found much support for Krishnamurti's theory. A reason for the discrepancy will be given in section 11.

The earlier pioneering studies by Palm (1960), Busse (1967) and Krishnamurti (1968) on Rayleigh-Bénard convection have shown that processes inducing a curved *static* (= *in the absence of convection*) horizontal mean temperature profile, such as height-dependent diffusion coefficients and time-dependent boundary conditions, determine the planform. Mean large scale vertical motion also alters the static temperature profile. The common denominator emerging from these studies is the sign of curvature of the static temperature profile. In all these studies "open cells" (down-hexagons) occur when the greatest static thermal instability is located below, while "closed cells" (up-hexagons) occur when the greatest static thermal instability is located at the upper boundary. The quotation marks are used here to indicate that the studies on Rayleigh-Bénard convection have never really paid any attention to the differences in the areas covered by, respectively, the up- and the downdraught. Because of the clouds, this property is immediately evident in the case of atmospheric cellular convection. Indeed, it is precisely this property that has received the most attention in the meteorological literature. Helfand and Kalnay (1983), for instance, define an open cell as a cell in which the updraught is more intense and thinner than the downdraught. It is then possible to arrive at conclusions about the preference for open or closed cells on the basis of a model of *two-dimensional* convection.

An assumption which is generally made, and which is also made in this paper, is that the layer is tessellated

into a regular array of identical cells. This limits the possible planforms to parallel strips (rolls), triangles, squares, rectangles and hexagons. Rectangles are not very likely to occur, except when there is some horizontally asymmetric effect. Since this is not the case here, squares will be preferred over rectangles. But even squares do not seem to be very probable. One reason for this is the difficulty of defining the cell-boundary in the case of squares. Stuart (1964) defined the cell-boundaries as surfaces through which there is no in- or outflow and on which the vertical velocity has the same sign everywhere. If the up- and downdraughts are equal in intensity and area, the boundaries of one square cell will always possess four points at which the vertical velocity is zero. That is, there is an ambiguity in defining the cellular boundaries. The vertical velocity along the boundary will vary strongly. If up- and downdraught-areas are unequal (asymmetry) this problem will not occur, since there are now separate closed curves, $w = 0$ (see Stuart, 1964). However, this does not yield a very efficient "packing" of (up)(down)draughts. The most efficient packing of circular up(down)draughts will lead to a hexagonal cellular pattern.

It was stated above that the critical parameter coming out of the theoretical studies on the effect of different physical processes on the planform of convection is the sign of curvature of the static vertical temperature profile. This is also suggested by observations of convection in the atmosphere.

Many cases of open cellular convection occur during polar air outbreaks in which the convection layer moves over a sea-surface which increases in temperature with distance from the ice-pack or frozen continent. The increasing surface temperature has the effect of maintaining a curved horizontal mean *static* temperature profile with the greatest thermal instability below. Although it is not actually possible to observe this static temperature profile, because the convection-currents continually act to modify it, it should be possible in most cases to determine the sign of the curvature of the static part of the profile.

From a study of satellite photographs over a period of several years, Agee et al. (1973) deduced that open cells preferably occur to the east of continents over warm ocean currents, while closed cells tend to occur to the west of continents over cooler ocean currents.

All this suggests that open cells will occur when the static temperature profile is such that the greatest thermal instability is located below, while closed cells will occur when the greatest static instability is located above. This hypothesis will be tested by performing simulations with a numerical model of convection.

In the next four sections the model and method of solution will be described. Technical details will be delegated to appendices. The results of integrations will be described in sections 7 and 8, and discussed in section 9. These integrations provide support to the hypothesis stated above. Unfortunately, a numerical model can never "prove" a hypothesis but only support it. At the moment analytical treatment of this highly nonlinear problem seems far from feasible.

The present paper does not find its justification solely from the verification of the hypothesis stated above, which, incidentally, was also tested and verified by Veltishchev and Zhelnin (1974, 1975) (see also Matveev (1984)). These results have largely escaped the attention of the western meteorological community. The numerical experiments described below, however, point to a property of thermal convection which has, to the author's knowledge, never before received any attention, namely its extremely low toroidal degree under certain circumstances. This subject will be taken up in section 10. The present paper will be concluded with a discussion of the applicability of the model (results) to atmospheric convection (section 11).

3 The Model Problem

The model problem is convection between stress-free, perfectly conducting horizontal boundaries held at different temperatures. This idealization of atmospheric convection is chosen so as to permit the use of Fourier modes to represent the fields of temperature and motion, making the mathematical treatment easier. It must be noted, however, that the upper boundary in the atmosphere is free, not rigid. It is usually formed by an inversion. Convection can penetrate into this inversion and excite waves which propagate upwards and along the inversion (Clark et al., 1986). These important effects are ignored here. Likewise, the effect of a horizontal mean flow with shear, known to induce the formation of rolls (Asai, 1970a, b), will not be taken into account.

The basic equations governing the dynamic and thermal behaviour of a shallow layer (depth, h , in the order of 1 km or less) of fluid are those expressing conservation of momentum, energy and mass, including the Boussinesq approximation (see Spiegel and Veronis, 1960):

$$\frac{d\vec{v}'}{dt} = \frac{-1}{\rho_m} \nabla p' + g\alpha T' \hat{k} + \nu \nabla^2 \vec{v}' \quad (3.1)$$

$$\nabla \cdot \vec{v}' = 0 \quad (3.2)$$

$$\frac{dT'}{dt} = \Gamma \vec{v}' \cdot \hat{k} + \kappa \nabla^2 (T' - \bar{T}) \quad (3.3)$$

where \vec{v} is the fluid velocity, t is time, p the pressure, T the temperature, ρ the density, α the volumetric coefficient of thermal expansion, g the acceleration due to gravity, ν and κ the eddy-diffusivities of momentum and heat, respectively, \hat{k} is the unit vector in the vertical direction, c_p is the specific heat capacity at constant pressure. Γ is the deviation of the vertical temperature gradient of the initial hydrostatic reference state from the dry-adiabatic lapse rate, $-\gamma_d (= -g/c_p)$. Γ is positive when the temperature of the static state decreases more rapidly with height than the dry-adiabat. \bar{T} is the steady "static" temperature perturbation, maintained against diffusion by a steady heat source, or by another physical mechanism which operates independent of the convection. In this study \bar{T} is only dependent on z and will be treated as a free parameter. The behaviour of the model will be investigated as a function of the shape of the profile, $\bar{T}(z)$.

The reference state is assumed to be motionless: $\vec{v}_m = 0$. Therefore, in the following all primes attached to \vec{v} and its components will be dropped.

The eddy-diffusion in equations (3.1) and (3.3) are parameterizations for the effect on the calculated motion, of motions resulting from processes, such as stress at the lower boundary, which are not included in the model problem. Mean wind-shear and stress at the lower boundary generate turbulent eddies which exert a stress on the "large-scale" eddies which are generated by convection. According to the mixing-length theory (see e.g. Tennekes and Lumley, 1972) this stress acts as a diffusion of momentum and heat on the large-scale eddies. It is assumed that the turbulence, resulting from shear-stress, is isotropic and homogeneous. This strong idealization of the effect of turbulent dissipation is introduced partially to keep up the analogy with the Rayleigh Bénard problem and partially because there is so little known about this effect that it is difficult to prescribe a more sophisticated parameterization. We will return to this problem in section 11.

From eqs. (3.1) and (3.2) it is possible to derive an equation for the vertical component of the vorticity,

$$\zeta = \frac{\partial v}{\partial x} - \frac{\partial u}{\partial y}, \quad (3.4)$$

where u and v are, respectively, the x - and y - (horizontal) velocity components, and an equation for the time evolution of $\nabla^2 w$, where w is the vertical component of the velocity, thereby eliminating p' . Thus the flow-field is divided into a so-called poloidal part, associated with w , and a so-called toroidal part, associated with ζ .

In terms of the following units the length $\{L\}$, time $\{t\}$ and temperature $\{T\}$,

$$\{L\} = h; \quad \{t\} = \frac{h^2}{\kappa}; \quad \{T\} = \frac{\kappa \nu}{g \alpha h^3}, \quad (3.5)$$

the vorticity equation is

$$\frac{d\zeta}{dt} = \zeta \frac{\partial w}{\partial z} - \frac{\partial w}{\partial x} \frac{\partial v}{\partial z} + \frac{\partial w}{\partial y} \frac{\partial u}{\partial z} + \text{Pr} \nabla^2 \zeta, \quad (3.6)$$

where Pr is the Prandtl number ($= \nu/\kappa$). The equation for $\nabla^2 w$ is obtained as follows: differentiate the x-component of (3.1) with respect to x , the y-component of (3.1) with respect to y and the z-component of (3.1) with respect to z . By adding the three resulting equations and using (3.2) a Poisson equation for p' is obtained. After differentiating this equation with respect to z , taking the Laplacian (∇^2) of the z-component of (3.1) and subtracting the two resulting equations, one obtains, in terms of the units defined in (3.5),

$$\begin{aligned} \frac{d\nabla^2 w}{dt} = & \left(2 \frac{\partial^2 u}{\partial z^2} - 2 \frac{\partial^2 w}{\partial x \partial z} - \nabla^2 u \right) \frac{\partial w}{\partial x} + \left(2 \frac{\partial^2 v}{\partial z^2} - \right. \\ & \left. - 2 \frac{\partial^2 w}{\partial y \partial z} - \nabla^2 v \right) \frac{\partial w}{\partial y} - \nabla^2 w \frac{\partial w}{\partial z} + \\ & + 2 \left(\frac{\partial^2 u}{\partial z \partial y} - \frac{\partial^2 w}{\partial x \partial y} \right) \frac{\partial v}{\partial x} + 2 \left(\frac{\partial^2 v}{\partial z \partial x} - \right. \\ & \left. - \frac{\partial^2 w}{\partial y \partial x} \right) \frac{\partial v}{\partial y} + 2 \left(\frac{\partial^2 u}{\partial z \partial x} - \frac{\partial^2 w}{\partial x \partial x} \right) \frac{\partial u}{\partial x} + \\ & + 2 \left(\frac{\partial^2 v}{\partial z \partial x} - \frac{\partial^2 w}{\partial x \partial y} \right) \frac{\partial u}{\partial y} + \text{Pr} \nabla_H^2 \theta + \text{Pr} \nabla^4 w. \end{aligned} \quad (3.7)$$

Here ∇_H^2 is the horizontal Laplacian, θ is the non-dimensional temperature deviation from the reference state. Except for ζ and w , eqs. (3.6) and (3.7) still contain the unknowns u and v . These can be eliminated, using eqs. (3.2) and (3.4) after the system has been Fourier transformed.

The nondimensional form of the temperature equation (3.3) is,

$$\frac{d\theta}{dt} = \text{Ra} w + \nabla^2 (\theta - \bar{\theta}), \quad (3.8)$$

where Ra is the Rayleigh number ($= g \alpha \Gamma h^4 / \nu \kappa$). The top and bottom boundaries (see Fig. 3) are assumed to be rigid, stress-free and perfectly conducting, i.e.

$$w = 0; \quad \frac{\partial u}{\partial z} = \frac{\partial v}{\partial z} = 0; \quad \theta = 0; \quad \frac{\partial^2 \theta}{\partial z^2} = 0, \quad (3.9)$$

at $z = 0$ and $z = 1$ (we are now expressing every variable

in terms of non-dimensional units (3.5)). The second condition in combination with (3.2) implies that

$$\frac{\partial^2 w}{\partial z^2} = 0 \quad \text{at } z = 0 \quad \text{and } z = 1. \quad (3.10)$$

These boundary conditions permit Fourier normal mode solutions in the vertical.

4 Fourier Representation

We will take the hexagonal convection cell as the prototype of an atmospheric convection cell. According to Christopherson (1940), a hexagonal pattern is given by,

$$\cos \sqrt{3} x \cos y \pm \frac{1}{2} \cos 2y. \quad (4.1)$$

Figure 1 shows a contour plot of a hexagonal cellular pattern according to this formula. The sign in front of the second term determines the direction of the vertical motion in the middle of the cell. The planform of the vertical motion in the middle of the cell is circular and is smaller in size than the vertical motion in the periphery. This may, however, change if higher harmonics are excited due to the interaction of the two "fundamental" waves which comprise (4.1).

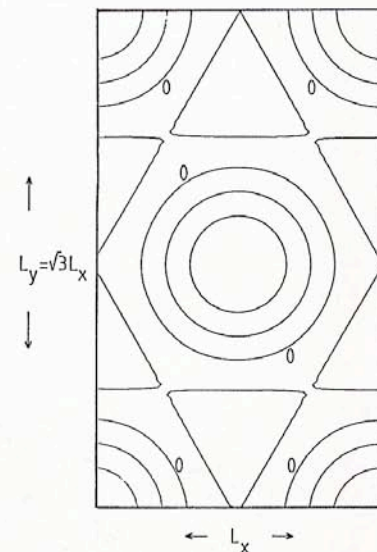


Figure 1 The vertical motion in a hexagonal cell according to formula (4.1). Along the contours labeled zero, the vertical velocity is zero. A "up-hexagon" is defined as a hexagonal cell in which the motion is upwards in the centre. In the case of a down-hexagon, the opposite is the case.

Let us write the variables in the form of Fourier series as follows:

$$\begin{bmatrix} u \\ v \\ w \\ \xi \\ \theta \\ \bar{\theta} \end{bmatrix} = \sum_{\alpha} \begin{bmatrix} U_{\alpha} \\ V_{\alpha} \\ W_{\alpha} \\ Z_{\alpha} \\ \Theta_{\alpha} \\ \bar{\Theta}_{\alpha} \end{bmatrix} S_{\alpha}(x, y, z), \quad (4.2)$$

where U_{α} , V_{α} , W_{α} , Z_{α} , Θ_{α} , $\bar{\Theta}_{\alpha}$ are complex coefficients, and

$$S_{\alpha}(x, y, z) = \exp \{ i\pi (a_x l_{\alpha} x + a_y m_{\alpha} y + n_{\alpha} z) \}. \quad (4.3)$$

The notation is exactly as in Kuo and Platzman (1961). \sum_{α} means a sum over all integral lattice points in the volume of $\alpha = (l_{\alpha}, m_{\alpha}, n_{\alpha})$. The parameters a_x and a_y are a measure of the horizontal domain of computation:

$$0 \leq x \leq L_x/h; \quad 0 \leq y \leq L_y/h, \quad (4.4)$$

so that

$$a_x = 2h/L_x; \quad a_y = 2h/L_y. \quad (4.5)$$

Because periodic boundary conditions have been assumed, this domain may be repeated in all horizontal directions ad infinitum, so as to obtain a regular array of cells with a prescribed wavelength.

If we choose

$$a_x = \sqrt{3} a_y \equiv \sqrt{3} a, \quad (4.6)$$

then the wave vectors, $(\pm 1, \pm 1, n)$ and $(0, \pm 2, n)$ (where n is an integer) correspond to the two modes in (4.1).

5 The Spectral Form of the Equations

The orthonormality of the S_{α} may be expressed in the form,

$$\int S_{\alpha} S_{\beta}^* d\sigma = \delta_{\alpha, \beta}, \quad (5.1)$$

where the asterisk designates a complex conjugate, while δ is the Kronecker delta. The integration extends over the region, $0 \leq x \leq 2/a_x$, $0 \leq y \leq 2/a_y$, $0 \leq z \leq 2$ and $d\sigma$ is a volume element divided by the total volume, $\sigma = 8/(a_x a_y)$.

The linear diagnostic relations (3.2) and (3.4) (which, incidentally, do not change when written in non-dimensional form) are thus easily transformed to spectral space. Substitution of (4.2) into (3.2) and (3.4) yields (after some rearrangements):

$$U_{\alpha} = \frac{-a_x n_{\alpha} l_{\alpha}}{q_{\alpha}^2} W_{\alpha} + \frac{a_y m_{\alpha}}{\pi q_{\alpha}^2} i Z_{\alpha}, \quad (5.2a)$$

$$V_{\alpha} = \frac{-a_y n_{\alpha} m_{\alpha}}{q_{\alpha}^2} W_{\alpha} - \frac{a_x l_{\alpha}}{\pi q_{\alpha}^2} i Z_{\alpha}, \quad (5.2b)$$

where $q_{\alpha}^2 = a_x^2 l_{\alpha}^2 + a_y^2 m_{\alpha}^2$ is the total horizontal wave-number. The total wavenumber is defined as,

$$k_{\alpha}^2 \equiv \pi^2 (q_{\alpha}^2 + n_{\alpha}^2). \quad (5.3)$$

With the help of eqs. (5.2a, b) U and V can be expressed in terms of Z and W . Therefore the motion-field is completely determined by the toroidal part (Z) and the poloidal part (W).

Transforming the prognostic equations (3.6–8) is a matter of substituting the expansions (4.2) into these equations and using the property of orthonormality of the S_{α} (5.1) to project the result on an arbitrary wave vector, $\gamma = (l_{\gamma}, m_{\gamma}, n_{\gamma})$. We then obtain a system of equations for the amplitudes W_{γ} , Z_{γ} and Θ_{γ} corresponding to an arbitrary wave vector, γ . This process requires some tedious but straightforward algebra, which is described in more detail in van Delden (1987). The spectral form of the equations is

$$\frac{dZ_{\gamma}}{dt} = \sum_{\alpha, \beta} F_Z(W_{\alpha}, Z_{\alpha}, W_{\beta}, Z_{\beta}, \alpha, \beta, \gamma) - \text{Pr } k_{\gamma}^2 Z_{\gamma}; \quad (5.4a)$$

$$\frac{dW_{\gamma}}{dt} = \sum_{\alpha, \beta} F_W(W_{\alpha}, Z_{\alpha}, W_{\beta}, Z_{\beta}, \alpha, \beta, \gamma) + \frac{\pi^2 q_{\gamma}^2}{k_{\gamma}^2} \Theta_{\gamma} - \text{Pr } k_{\gamma}^2 W_{\gamma}; \quad (5.4b)$$

$$\frac{d\Theta_{\gamma}}{dt} = \sum_{\alpha, \beta} F_{\Theta}(\Theta_{\alpha}, W_{\beta}, Z_{\beta}, \alpha, \beta, \gamma) + \text{Ra } W_{\gamma} - k_{\gamma}^2 (\Theta_{\gamma} - \bar{\Theta}_{\gamma}), \quad (5.4c)$$

where $\sum_{\alpha, \beta}$ is a double sum over all wave-vectors, α and β . F_Z , F_W and F_{Θ} are complicated nonlinear expressions which are given in appendix A. $\bar{\Theta}_{\gamma} = 0$ unless $l_{\gamma} = m_{\gamma} = 0$.

Equations (5.4a, b, c) have to be truncated in spectral space before numerical integration is feasible. To save computer resources, a highly truncated system (a so-called low-order model) is integrated from the rest-state to a steady state. This steady state is inserted into a more complete model (with more Fourier coefficients) and the integration is continued until a new, probably more realistic (steady) state is reached.

In the *low order model* the following wave vectors are taken inside the truncation of the expansion of w and θ : $(\pm 1, \pm 1, \pm n)$ and $(0, \pm 2, \pm n)$, $n = 1, 2$. In addition to this, $(0, 0, \pm n)$ where $n = 1, 2, 3, 4$ is taken to rep-

represent the mean vertical temperature profile. Only the imaginary parts of W and Θ (W^I and Θ^I) are taken into account. The low-order model equations are given explicitly in appendix C.

In the *higher-order model*, the following wave vectors are included inside the truncation of Z_γ , W_γ and Θ_γ (*imaginary and real*): $-6 \leq m_\gamma \leq 6$, $-3 \leq l_\gamma \leq 3$, $-3 \leq n_\gamma \leq 3$ (except $n = 0$), in addition to $(0, 0, \pm n)$ ($4 \leq n \leq 6$) for the temperature profile. In "physical space" this would correspond to a grid of 7×11 points in the horizontal and 7 in the vertical to describe the waves, and 11 in the vertical to describe the vertical mean temperature profile. However, with the present spectral method we need not worry about numerical diffusion or nonlinear numerical instability. This truncation seems adequate enough to simulate convection cells with an aspect ratio equal to $2\sqrt{2}$ (the linearly preferred value (Rayleigh (1916)) at $Ra \leq 5000$ (eight times the critical value for onset). This is based among other on a comparison of the heat transport produced by the present model with heat transports found in other computations reported in the literature (see van Delden, 1987).

6 The Imposed Static Temperature Profile

The principle purpose of this study is to see how the planform of convection is sensitive to changes in the imposed static temperature profile. We will limit the investigation to a particular shape of the static temperature profile. To this end the Fourier expansion of $\bar{\Theta}$ is truncated after the first term. The boundary condition (3.9) and the fact that $\bar{\Theta}$ is real, imply that the

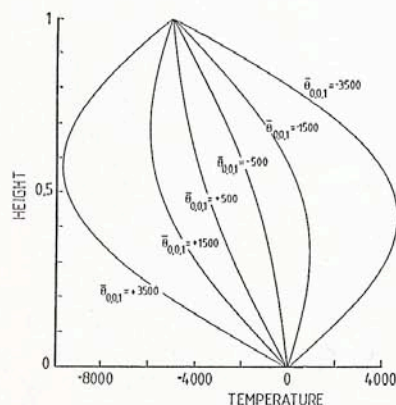


Figure 2 The static temperature profiles, relative to the dry-adiabat and the temperature of the lower boundary, for several values of $\bar{\Theta}_{001}$. The units of height and temperature are dimensionless ($Ra = 5000$).

static temperature profile is determined by one Fourier coefficient, namely $\bar{\Theta}_{0,0,1}^I$ (see appendix B). The superscript, I , as well as the commas in the subscript will henceforth be dropped. Figure 2 gives an impression of the static temperature profile as a function of $\bar{\Theta}_{001}$. When $\bar{\Theta}_{001} = 0$ (i.e. the static temperature profile is rectilinear) the static state becomes unstable at minimum $Ra = 657$. Kondo et al. (1972) investigated the stability of the static state in the presence of the temperature profiles shown in Figure 2. They found that the critical Rayleigh number for onset of convection decreases slightly from 657 to 654 if $\bar{\Theta}_{001} = \pm 500$ ($T_1 = 0.2$ in their paper), to 636 if $\bar{\Theta}_{001} = \pm 1500$, and 536 if $\bar{\Theta}_{001} = \pm 3500$. The corresponding critical (preferred) wavenumber increases by a maximum of 7% at $\bar{\Theta}_{001} = \pm 3500$.

7 Planform-Selection According to the Low-Order Model

Figure 3 shows the time-evolution of the temperature Fourier coefficients Θ_{111}^I and Θ_{021}^I in an integration with the low-order model starting from rest (perturbed randomly), with $Pr = 0.025$, $Ra = 5000$, $a = 1/2\sqrt{2}$ and $\bar{\Theta}_{001} = 0$. If $\bar{\Theta}_{111}^I = \bar{\Theta}_{021}^I$, the planform is hexagonal, as in Figure 1. If $\bar{\Theta}_{111}^I = 0$ and $\bar{\Theta}_{021}^I \neq 0$, the planform is two-dimensional (rolls). Evidently the planform is hexagonal for a rather long time-period of 13 units, after which there is a sudden transition to rolls. Such behaviour was also observed in laboratory-

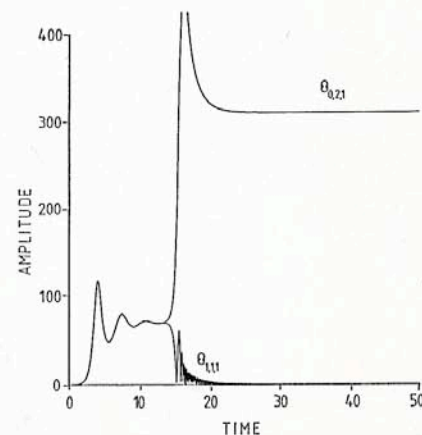


Figure 3 The absolute value of the coefficients, Θ_{021} and Θ_{111} , as a function of time in a run with the low order model of three-dimensional poloidal convection. Until $t = 13$ units, the coefficients are exactly equal, corresponding to a hexagonal planform. After that Θ_{111} goes to zero, marking the transition to rolls. The parameter values are, $Pr = 0.025$, $a = 1/(2\sqrt{2})$ and $Ra = 5000$.

experiments performed by Gollub et al. (1982). In these experiments certain convection patterns persisted for a long time, but eventually gave way to another, probably more stable, convection pattern.

More integrations with the low-order model were done with $\Theta_{001} = 0$. The initial conditions were given by perturbing the temperature wave field (Θ_{111}^I , Θ_{112}^I , Θ_{021}^I , Θ_{022}^I) with a preset value (s) with a sign determined by the random generator. All other coefficients were equal to zero initially. The integrations were continued until a steady state was reached. At low Pr care had to be taken in assuring that the solution was steady, because, as illustrated in Figure 3, almost invariably the system seemed to select and stick to a hexagonal solution for a long time and yet then, quite abruptly, select the roll solution. Table 1 shows the solutions obtained for different values of s and Pr at $Ra = 5000$ and $a = 1/2\sqrt{2}$. Apparently, there is a preference for hexagons at high Pr and for rolls at low Pr.

The most remarkable result of these integrations is that an asymmetric (hexagonal) planform is selected in perfectly symmetric conditions, even though there is the possibility of selecting a symmetric (roll) planform. Because of their asymmetry, hexagons have always been thought to result only when an asymmetry is imposed on the system, such as a curved static temperature profile. The low-order model-behaviour suggests that this physical reasoning is incorrect. It is true that the stability analyses by Busse (1967) and Krishnamurti (1968) indicate that imposed asymmetries promote the stability of hexagonal convection. How-

Table 1 Solution of the low-order model after 50 time units as a function of initial conditions (s) and Prandtl number (Pr) at $Ra = 5000$ and $a = 1/2\sqrt{2}$. For low Pr (0.025 and 0.2) the quasi-steady or time dependent solutions after 10 and 3 time-units, respectively, are shown. S = square or, more precisely, a rectangle; R = roll; D = down-hexagon; U = up-hexagon; T = time-dependent solution (wavy roll). The asterisk denotes that the solution is not exactly a hexagon. The solutions chosen as initial condition for the higher-order numerical model are printed in italic (see section 8).

Pr →	0.025		0.2		1	5	50
time →	10	50	3	50	50	50	50
s							
0.25	T	R	T	S	<i>D*</i>	<i>D</i>	D
0.5	U	R	U	R	R	U	U
1	U	R	U	R	R	U	U
2	U	R	U	R	R	U	U
4	T	R	R	R	R	D	D
8	U	R			R		U
16	U	R			R		U
32	T	R			R		U
64	U	R			R		U
128	T	R			<i>D*</i>		D
256	D	R			R		D

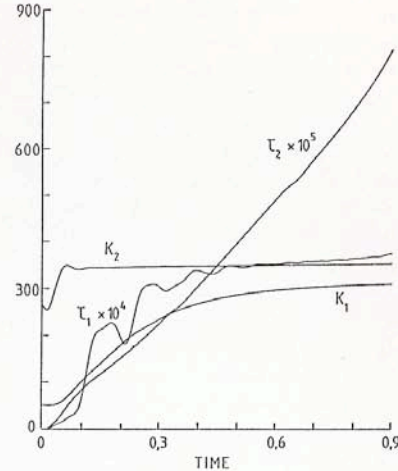


Figure 4 The kinetic energy, K , and the toroidal degree, τ , as a function of time (all dimensionless) for, (a) runs 1 ($Pr = 0.2$) and 2 ($Pr = 1$). The subscripts of K and τ refer to the run-number in Table 3.

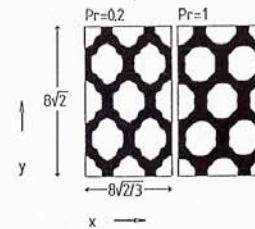


Figure 5 Planforms in terms of the vertical velocity at $z = 4/7$ at the end of runs 1 and 2 (see Table 3). White corresponds to positive vertical motion whereas black corresponds to negative vertical motion. The only parameter that is varied is the Prandtl number, Pr (see Table 3). Units are dimensionless.

ever, it also seems from the photographs taken by Krishnamurti (1970, Fig. 5) that hexagons are possible in symmetric conditions (rectilinear static temperature profile), although Krishnamurti only alludes to the mere three-dimensionality of the flow in these cases. Besides, so-called "spoke-pattern" convection, which is observed in symmetric conditions (Busse, 1978), possesses the same kind of asymmetry as hexagonal convection.

It must be remarked that perfectly symmetric conditions are probably impossible to produce perfectly in the laboratory. Deviations from the Boussinesq approximation, for example, will induce asymmetries. In this context it should be noted that at $Pr < 1$, the hexagon is unstable and gives way to a roll (see Fig. 3), whereas at $Pr > 1$ the hexagon is stable within the

framework of the low-order model. Both up- and down-hexagons are equally probable. At $Pr = 1$ the hexagon is never selected. Only in two cases ($s = 0.25$ and $s = 128$) did the model select a three-dimensional steady solution, which resembles a compromise between a rectangle and a hexagon. These results lead one to wonder whether the unequal magnitudes of the heat diffusion- and momentum diffusion-coefficients when $Pr \neq 1$ also act as an internal asymmetry which can influence the planform selection.

Let us now see what happens when a curved static temperature profile is imposed on the system. For each set of parameter-values a set of six integrations of 20 time units, with different s , was performed. Table 2 shows the selected solutions as a function of Ra and $\bar{\Theta}_{001}$. Several solutions are possible at the same parameter-values. Most remarkable is that up-hexagons and rolls are preferred when $\bar{\Theta}_{001} > 0$ (greatest static instability below), while down-hexagons and rolls are preferred when $\bar{\Theta}_{001} < 0$ (greatest static instability above). With respect to the relative areas occupied by the up- and down-draught, this result is in agreement with the findings of Helfand and Kalnay (1983), since the motion in the middle of the low-order model hexagon *always* covers a smaller horizontal area than the vertical motion in the periphery (see Fig. 1).

8 Planform Selection According to the Higher Order Model

To relax this constraint on the internal structure of the cell, higher harmonics must be included in the model. Therefore, a poloidal down-hexagon (or up-

hexagon) with an aspect ratio of $2\sqrt{2}$ (more specifically, the low-order model solution (D or U) at $Ra = 5000$, $a = 1/2\sqrt{2}$, $Pr = 0.2$ or 5 , printed in italic in Table 1 (for the runs at $Pr = 1$, the solutions at $Pr = 5$ in Table 1 were used)) was inserted into the higher-order model as initial condition and the integrations were continued for several values of $\bar{\Theta}_{001}$. Table 3 gives a survey of the integrations discussed in this paper.

In runs 1 and 2, differing only with respect to the Prandtl number, the initial condition was an up-hexagon (U). The static temperature profile was rectilinear. Figure 4 shows the time-evolution of the total kinetic energy K and the toroidal degree $\tau = K_T/K$, where K_T is the total kinetic energy associated with the toroidal part of the flow (Z) (see appendix D for exact definitions) for runs 1 and 2. According to the stability theory of Schlüter et al. (1965) for *small amplitudes* the hexagon should be unstable to infinitesimal perturbations. After 0.9 time units of integration, which corresponds to about 9 hours if $\kappa = 30 \text{ m}^2/\text{s}$ and $h = 1000 \text{ m}$, the system has indeed not reached a steady state. However, considering the planform is still hexagonal (see Fig. 5) after this time, it must be concluded that, within the framework of this model, the degree of instability of the hexagon is not very great.

Note that less than 1% of the total kinetic energy becomes toroidal when $Pr = 1$. Even when $Pr = 0.2$, τ is never greater than 0.037. This implies that the flow is nearly poloidal. We will return to this remarkable fact later.

Meanwhile we will discuss the influence of the (sign of the) curvature of the static temperature profile. In this context the integrations at $\bar{\Theta}_{001} = 1500$ (run 3) and at $\bar{\Theta}_{001} = -1500$ (run 4) are especially instructive

Table 2 Solutions (D/R/U) of low-order model integrations with random initial conditions (see text) as a function of Ra and $\bar{\Theta}_{001}$, which represents the degree and sign of curvature of the static temperature profile ($Pr = 3$ and $a = 1/(2\sqrt{2})$). For example, out of the six runs made at $Ra = 2500$ and $\bar{\Theta}_{001} = -8000$, the model selected a down-hexagon (D) three times and a roll (R) the other three times, while an up-hexagon (U) was never selected. At $Ra = 10000$ and $\bar{\Theta}_{001} = 0$, the model-behaviour is time-dependent (T) five times.

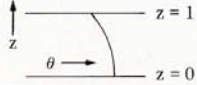
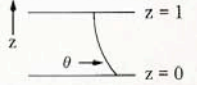
Ra	$\bar{\Theta}_{0,0,1}$						
	-8000	-5000	-2000	0	2000	5000	8000
2500	3/3/0	6/0/0	3/3/0	1/1/4	0/1/5	0/1/5	0/1/5
5000	3/3/0	2/4/0	2/4/0	2/0/4	0/1/5	0/1/5	0/1/5
10000	3/3/0		4/2/0	0/0/1 5 × T	0/2/4		0/1/5
Form of the static temperature profile							

Table 3 Summary of the 15 runs made with the higher-order model ($a = 1/(2\sqrt{2})$, $Ra = 5000$). C (cloud cover; see text for definition) and τ (the toroidal degree) are measured at the end of the run after Δ time units. "Stationary" implies that τ and K must be approximately constant for at least 0.1 time units. U = up-hexagon; D = down-hexagon; R = roll; I = irregular pattern.

Run no.	$\bar{\Theta}_{001}$	Pr	Δ	initial planform	final planform	stationary?	C	τ
1	0	0.2	0.9	U	U	NO	0.59	$3.7 \cdot 10^{-3}$
2	0	1	0.9	U	U	NO	0.53	$8.1 \cdot 10^{-4}$
3	1500	1	0.6	D	D	YES	0.43	$2 \cdot 10^{-3}$
4	-1500	1	0.9	D	R	NO	0.59	$1.8 \cdot 10^{-3}$
5	1500	1	0.6	U	R	NO	0.41	$1.9 \cdot 10^{-3}$
6	3500	1	0.6	D	R	NO	0.41	$1.9 \cdot 10^{-2}$
7	-3500	1	0.6	D	U	NO	0.58	$1.0 \cdot 10^{-2}$
8	500	1	0.3	D	D	NO	0.44	$1.9 \cdot 10^{-3}$
9	-500	1	0.6	D	R	NO	0.49	$1.5 \cdot 10^{-2}$
10	3500	5	0.6	D	I	NO	0.41	$5.5 \cdot 10^{-4}$
11	-3500	5	0.3	D	I	NO	0.58	$12.8 \cdot 10^{-4}$
12	0	5	0.3	D	D	YES	0.46	$9.6 \cdot 10^{-6}$
13	-5000	5	0.3	D	I	NO	0.62	$2.2 \cdot 10^{-3}$
14	2500	5	0.3	D	D	YES	0.42	$1.6 \cdot 10^{-4}$
15	3500	1	0.9	R	I	NO	<0.5	$1.7 \cdot 10^{-2}$

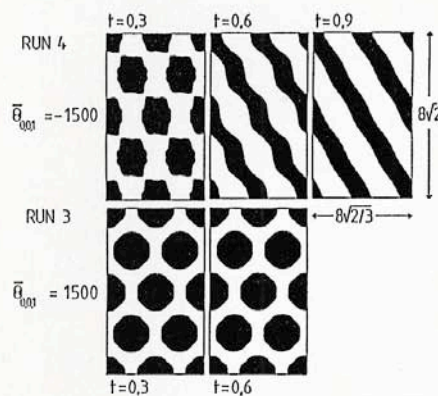


Figure 6 Vertical velocity (white: positive; black: negative) at $z = 4/7$ at different time in run 3 and run 4 (see Table 3). The initial condition is a down-hexagon, which evidently is only able to subsist when $\bar{\Theta}_{001} = 1500$. Units are dimensionless.

to compare. In both cases, the initial condition was a down-hexagon (D). Figure 6 shows the planforms, in terms of the vertical velocity at $z = 4/7$ at different times for both integrations. For a better overall picture, the domain of computation is extended half a wavelength in each direction. This will be done every time in this section. Apparently, the down-hexagon subsists when $\bar{\Theta}_{001} = +1500$ (greatest instability below), while it does not subsist when $\bar{\Theta}_{001} = -1500$. In the latter case there is a gradual transition to a roll pattern. Evidently, the "cloud-cover", C, which is defined as the vertically averaged ratio of the hori-

zontal updraught-area to the total horizontal cell-area, has adjusted to the sign of curvature of the temperature profile. When the layer is most unstable below, the cloud-cover is low, which is in agreement with the low-order model-results and the two-dimensional model results of Helfand and Kalnay (1983). However, the cell-circulation-direction is the reverse of that predicted by the low-order version of the model. The resulting stationary state convection cell closely resembles an atmospheric open convection cell, i.e. a down-hexagon with a large "clear" area (downward motion) in the middle.

To test the reliability of these results, another run (5) was done at $\bar{\Theta}_{001} = 1500$ with an up-hexagon ("U" at $s = 0.5$ and $Pr = 5$ in Table 1) as initial condition. As expected from the symmetry of the problem, the up-hexagon cannot subsist. There is a transition to rolls.

Figure 7 shows the mean vertical temperature stratification (static + dynamic) at the end of runs 3 and 4. In run 3 the static temperature stratification is stable near the upper boundary. Convection destroys this stable layer and converts into an unstable layer. This ensures that no heat accumulates inside the layer, i.e. that the net heat flux out of (into) the domain is equal to the prescribed heating (cooling) rate maintaining the curved static temperature profile.

The temperature profiles in Figure 7 also illustrate the unrealistic character of the upper boundary condition on the temperature in relation to the atmosphere, where convection never creates an unstable stratification at the top because it is allowed to penetrate further into the stable layer above.

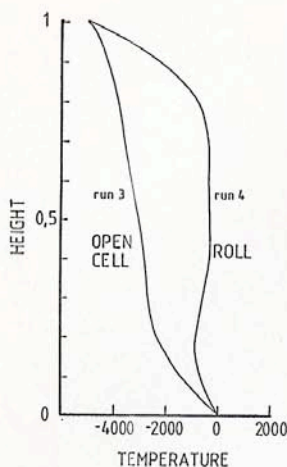


Figure 7
The mean vertical temperature profiles relative to the dry adiabat at the end of runs 3 and 4 (see Table 3). Units are dimensionless.

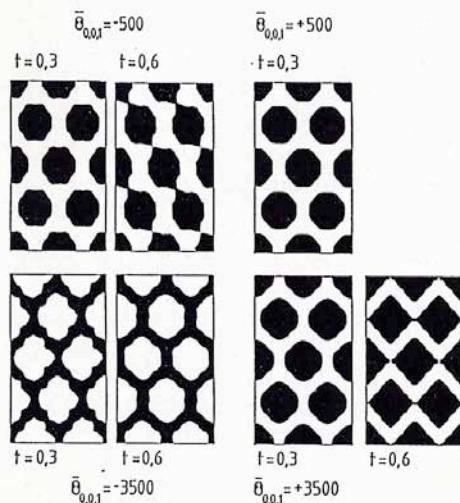


Figure 8 As Figure 6, except for runs 6 ($\bar{\Theta}_{001} = 3500$), 7 ($\bar{\Theta}_{001} = -3500$), 8 ($\bar{\Theta}_{001} = 500$) and 9 ($\bar{\Theta}_{001} = -500$). The initial condition is a down-hexagon in all cases (see Table 3 for further information).

Four more integrations were performed for different values of $\bar{\Theta}_{001}$, with exactly the same initial condition as in runs 3 and 4. Figure 8 shows the planforms in terms of the vertical velocity at $z = 4/7$. Most remarkable is that at $\bar{\Theta}_{001} = -3500$ the cell circulation direction has been reversed. The "cloud-cover" is 0.58. This convection pattern thus resembles a closed cell in the atmosphere.

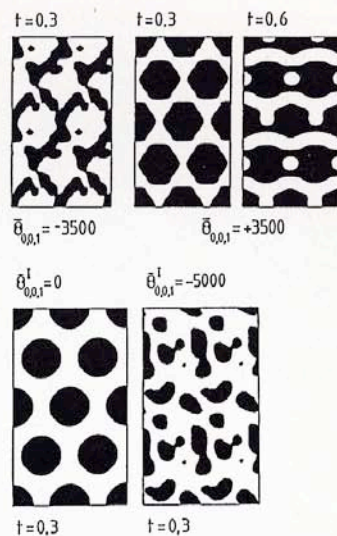


Figure 9 As Figure 6, except for runs 10 ($\bar{\Theta}_{001} = 3500$), 11 ($\bar{\Theta}_{001} = -3500$), 12 ($\bar{\Theta}_{001} = 0$) and 13 ($\bar{\Theta}_{001} = -5000$). See Table 3 for further information.

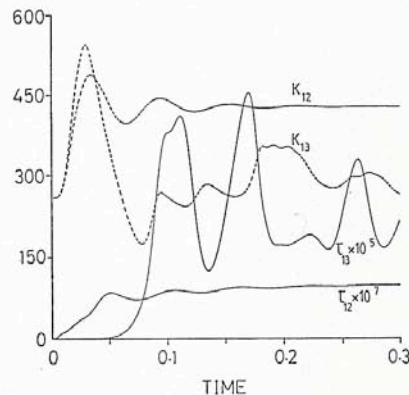


Figure 10 The kinetic energy, K , and the toroidal degree, τ , as a function of time in runs 12 and 13. Units are nondimensional. See Table 3 for further information.

Another set of five integrations was performed at $Pr = 5$ (runs 10–14). This should give an impression of the influence of the Prandtl number on the planform. Figure 9 shows the planforms at the end of runs 10–13. In symmetric conditions ($\bar{\Theta}_{001} = 0$, run 12) the hexagon persists for 0.3 time units at $Pr = 5$ (see Figure 10), which seems inconsistent with the small-amplitude stability theory of Schüster et al. (1965),

which predicts that hexagons are unstable. There is, however, a possibility of a sudden transition to another solution after a long time, as illustrated in Figure 3 for the low-order model. But, to simulate 13 time units would require about 120 hours Central Processor Unit time on the CYBER 180/855. Since the model-behaviour at time scales of about 0.3–0.9 time units (several hours in the atmosphere) is consistent with the analytical stability analyses of Busse (1967), Krishnamurti (1968) and the numerical results of Veltishchev and Zhelnin (1975), this special point in parameter space which, due to the inevitable presence of asymmetries in reality, will actually never occur, will not be investigated further. It is perhaps worth mentioning in this context that a recent study by de Swart and Grasman (1987) has shown that a nonlinear system may remain in the neighbourhood of a linearly unstable equilibrium for some time due to the fact that it may be attracted to this equilibrium in all directions of phase space, except one.

On the whole it seems that the increase of Pr stabilizes the flow in symmetric conditions, but destabilizes the flow in asymmetric conditions (e.g. compare the planforms in runs 7 and 11).

Figure 11 shows a detailed view of the vertical velocity at $z = 4/7$ in the steady state "open" cell at the end of run 29, in which convection was driven from below. The maximum upward velocity in the periphery is 47 nondimensional units, whereas the maximum downward velocity in the centre is 30 nondimensional units. There are six peaks in the upward motion in the periphery, while the downward motion has only one peak. This brings us to another remarkable property of open cells in the atmosphere, namely that, apart from a large clear area in the centre, they consist of a ring of many clouds, each with their own up- and downdraughts. Due to this, Scorer (1986) called these cells "beaded cells". The cell in Figure 11 reproduces this property to a certain extent. Each of the six updraught-peaks could be associated with a cloud (or bead).

It is somewhat enigmatic why the periphery is the "active" part of the cell, since this does not seem to be the most efficient organization in terms of protection against diffusive dissipation (see e.g. Oerlemans, 1986). Clearly, the convective planform-selection process defies an explanation in terms of optimum principles or symmetry arguments.

Finally, Figure 12 (run 15) is an illustration of the effect of the curvature of the static temperature profile on rolls. Initially a purely two-dimensional (roll) circulation is imposed. Apparently, there is a transition to a pattern in which updraughts are organized into "streets" with double the aspect ratio of the original

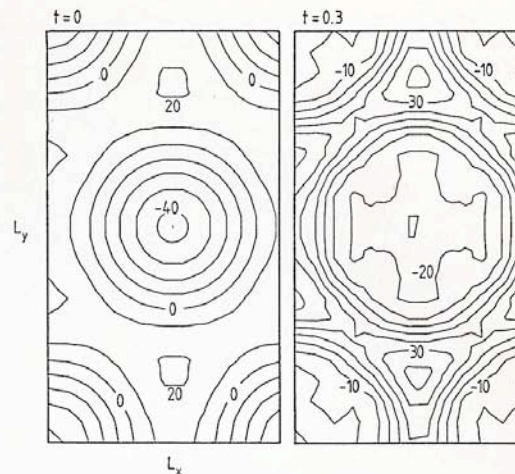


Figure 11 The vertical velocity at $z = 4/7$ in nondimensional units at the beginning and at the end ($t = 0.3$) of run 14 ($Ra = 5000$, $a = 1/(2\sqrt{2})$, $Pr = 5$, $\Theta_{001} = 2500$, $L_x = 4\sqrt{2/3}$ and $L_y = 4\sqrt{2}$). See Table 3 for further information.

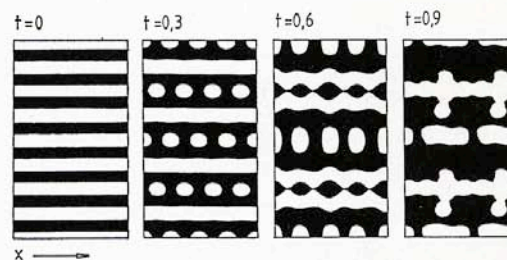


Figure 12 Vertical velocity (white: positive; black: negative) at $z = 4/7$ at different times in a run (15) (see Table 3) with rolls aligned in the x -direction as initial conditions. Some rolls (continuous cloud-lines; white in the figure) break up into discontinuous cloud lines or "cloud-streets".

roll, much in the same way as is observed in the atmosphere (e.g. Weston, 1980).

9 Discussion and Conclusions on Planform-Selection in the Model

A survey of all the higher order model integrations, and their implication and validity, is now possible. The main result is that *varying static thermal stability determines the cell circulation direction and cloud-cover*. Roughly stated, open cells occur when static instability is greatest adjacent to the lower boundary, while closed cells occur when the static instability is greatest adjacent to the upper boundary.

It is expected that this conclusion is valid for all Rayleigh numbers below 5000 and above 657, which is the minimum value needed for onset of convection, as well as for values of the wave number, a , in the vicinity of the chosen value, which is the preferred wave number according to linear theory without rotation. For lower wave numbers, which are frequently observed, more higher harmonics are needed inside the truncation. There is, however no physical reason to believe that the cell circulation direction will reverse, or that the cloud-cover will differ significantly when a is smaller and/or when Ra is larger than the chosen value, but this remains to be tested with higher resolution integrations on a super-computer.

The earth's rotation was ignored in this paper. Nevertheless, runs with rotation (oriented parallel to the local vertical), described in van Delden (1987), show a very similar model behaviour for rotation-rates applicable to the atmosphere. However, there is more to this problem than is evident at first sight, since the rotation vector at latitudes other than 90° is tilted to the vertical. In that case the Fourier modes $Z_{l,m,0}$, which were left outside the truncation, should certainly be included.

As to the sinusoidal form of the static temperature profile, it was chosen in part due to its mathematical simplicity, and also due to the fact that it resembles the basic characteristics of the static temperature profile encountered in the atmosphere. Previously, Krishnamurti (1968) and Veltishchev and Zhelnin (1975) investigated a (similar) parabolic profile and obtained identical qualitative results. This indicates that the results are not greatly sensitive to the specific form of the static temperature profile, but much more to the sign of the variation of the static stability and where, relative to the upper and lower boundaries, the maximum static instability is located.

Finally, Figure 13 presents a strongly tentative regime diagram in $Ra-\Theta_{001}$ space at $a = 1/2\sqrt{2}$ and $Pr \approx 1$ to 5, distilled from the model integrations described in section 8 and also results due to Busse (1967) and Krishnamurti (1968, 1975a). The line separating the static state from convection is taken from the paper by Kondo et al. (1972). A more exact determination of this regime diagram, also at other wavelengths, is a matter of the availability of computer-time.

10 The Toroidal Component of the Flow

The last column in Table 3 shows the toroidal degree at the end of each model-run. It is very remarkable that this quantity is very small in all cases. More than 99% of the energy is poloidal. This would permit us

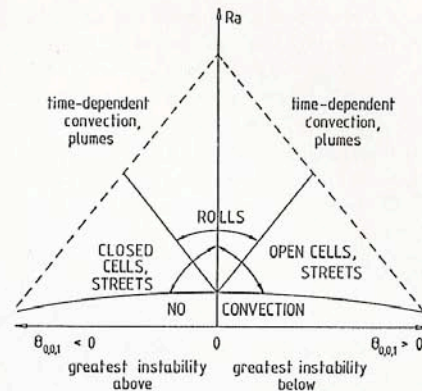


Figure 13 Tentative regime-diagram in $Ra-\Theta_{001}$ space, distilled from the numerical results, Krishnamurti's (1968, 1975) theory, and the stability analysis of the static state by Kondo et al. (1972). For the definition of "cloud streets", see Figure 12.

to neglect the toroidal component (Z) of the flow in the spectral equations of motion, which leaves us with a comparatively very simple equation with only one nonlinear term:

$$\frac{dW_\gamma}{dt} = \sum_{\alpha, \beta} \pi N_{\gamma\alpha\beta} i W_\alpha W_\beta + \text{linear terms.}$$

(see section 5 and appendix A). This equation is identical to the equation of motion for two-dimensional flow, except that the vector-summation covers the whole volume, while it is restricted to a plane ($l=0$ or $m=0$ or $n=0$) in the case of two-dimensional flow. The nonlinear dynamics of three-dimensional convection should therefore exhibit considerable similarity with two-dimensional flow.

The reason for the low toroidal degree of shallow convection in the absence of rotation and shear is principally due to the fact that, because the buoyancy force is directed in the vertical, thermal instability is manifest only in the poloidal modes of the Fourier spectrum of the flow field. The toroidal modes are all damped and can be excited only through the nonlinear coupling with the poloidal modes. It has been established by Haken (1978) that nonlinear systems in general are dominated by the amplified modes. The damped modes follow the amplified modes as slaves, which means that they are always in balance with the amplified modes. Haken (1978) called this "the slaving principle". At low Pr viscous dissipation will of course be less than at high Pr . Therefore at low Pr the motion will be more strongly toroidal.

There is another reason for the low toroidal degree. It is shown in appendix E that the interaction of two

poloidal Fourier modes with identical vertical wave number, n , and equal total horizontal wave numbers, q , does not produce any toroidal energy. All regular (symmetric) cells, such as hexagons and squares, consist mainly of two or more fundamental modes with the same total horizontal wave number, q . Therefore, these cellular patterns should possess an even lower toroidal degree than more irregular flow-patterns.

The curvature of the static temperature profile has no direct influence on the toroidal component of the flow (and vice-versa), as is shown in appendix E. Therefore, the toroidal component of the flow should not influence the planform selection process. This was verified by repeating runs 3 and 4 with $Z_\gamma = 0$ for all γ . With this constraint, the model behaviour is nearly identical.

A separate paper will be devoted to the dynamical properties of (three-dimensional) poloidal flow.

11 Parameter Values and the Applicability of the Model to the Atmosphere

The problem of the applicability of the model to the atmosphere becomes clearly evident when one tries to determine the values of the nondimensional parameters, Ra and Pr in the atmosphere. It appears that this is especially the case with the Rayleigh number. Actually one has to determine two Rayleigh numbers: a moist Rayleigh number, Ra_m , where the atmosphere is saturated with water-vapour, and a dry Rayleigh number, Ra_d , where the atmosphere is not saturated. Although everyone is aware of this problem, it is usually ignored. In many studies, where the effects of latent heat release are otherwise neglected, one or a mean value of the two Rayleigh numbers is taken when comparing the theory with reality. But even then there is the problem of determining the top of the convective layer. The upper boundary in the model is fixed, whereas in the atmosphere it is free. The question is whether the upper boundary coincides with the inversion base or, possibly, with the point at which the potential temperature is equal to the potential temperature at the ground. In the latter case the temperature-difference between the upper and the lower boundary, ΔT , is equal to zero, and therefore $Ra = 0$, that is, convection penetrates into the inversion until the layer is neutrally stable. The problem is illustrated in Figure 14. Walter (1980) and Weston (1980) use the inversion base as the top of the layer, while Miura (1986) estimates the cloud-top height from satellite and rawinsonde data, finding it to be greater than the inversion-base height. Obviously, the mean potential temperature lapse rate in the layer, Γ , is then significantly lower. In

his observational study of rolls and cells to the east of the Asian continent, Miura (1986) finds that $4 \cdot 10^5 < Ra_m < 2 \cdot 10^6$ and $-4 \cdot 10^4 > Ra_d > -2 \cdot 10^6$, where he assumes that $\nu = 100 \text{ m}^2/\text{s}$ and $\kappa = 25 \text{ m}^2/\text{s}$ (i.e. $Pr = 4$). Therefore, the mean value of Ra_d and Ra_m , Ra , lies in the range $0 < Ra < 10^6$. If the three-dimensional numerical computations are to be compared with reality, it is best to take Ra as the relevant parameter. It is then seen that the numerical computations have been performed at relatively low Rayleigh numbers ($5 \cdot 10^3$).

The problem of determining the value of Pr in the atmosphere has been discussed shortly in section 3. In the literature on mesoscale cumulus convection there is very little discussion on this problem, probably because it is so elusive. More than with the problem of determining the Rayleigh number, it lies on the fundamental side of the model formulation. It is not very clear what is actually modelled. It is assumed that the eddies generated by mean wind shear near the lower boundary act dissipatively on the resolved flow, and that this goes analogous to a diffusion process of momentum and heat. All this is based on not very solid intuitive physical arguments. Even if this process can be modelled by diffusion terms, there remain many uncertainties about the diffusion coefficients of heat and momentum, their dependence on space, flow and direction and, finally, their ratio (i.e. Pr). Since the question of the value of Pr comes after so many other unanswered questions, everyone has evaded the problem and cited previous authors when fixing the Prandtl number in model calculations. Clearly, an investigation is needed into the exact nature of dissipation affecting convection currents in the atmosphere.

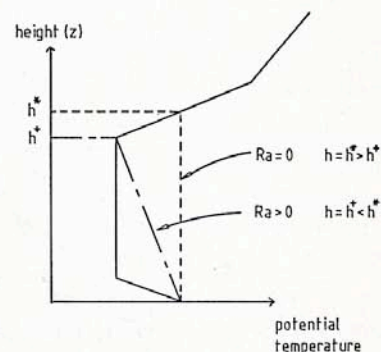


Figure 14 Two possible upper boundaries, $z = h^*$ and $z = h^+$, to convection in the atmosphere. The solid line is a representative potential temperature profile. When the top-boundary is at $z = h^*$, $Ra = 0$. When the top-boundary is at the inversion base, $z = h^+$, $Ra > 0$.

The exact value of $\bar{\Theta}_{001}$ (the curvature of the static temperature profile) is, of course, impossible to determine in the atmosphere. But this is actually not a great problem, since it is only the sign of $\bar{\Theta}_{001}$ which we need. In this context a note on the effect of large-scale downward or upward motion on the static temperature profile is in place. Subsidence, for example, produces steady adiabatic warming if the stratification is conditionally unstable, and steady adiabatic cooling if the stratification is absolutely unstable. Since the bulk of the atmosphere is usually conditionally unstable, subsidence usually makes the parameter $\bar{\Theta}_{001}$ negative. Therefore closed cells should usually (in conditionally unstable conditions) be preferred when there is subsidence and not open cells, as Krishnamurti (1975b) predicted. The reason for the discrepancy is not that there is something wrong with Krishnamurti's (1975a) theory on the effect of large scale motion on planform selection, but that she tested this theory for an absolutely unstable atmosphere with two cases in which the atmosphere was conditionally unstable. *Only to the extent that it influences the vertical variation of the stratification, does mean vertical motion determine whether open or closed cells occur.*

Because the model is such a strong idealization of atmospheric shallow convection, the present investigation should be viewed more as a search for mechanisms, which can serve as an explanation of planform selection. This implies that, in relation to the atmosphere, the results should be viewed more qualitatively than quantitatively. The most important qualitative result is that open cells occur when convection is driven mainly from below, while closed cells occur when convection is driven mainly from above. This agrees with the climatology of Agee et al. (1973), in which open cells are mainly found over relatively warm oceans, while closed cells are found over oceans with a surface temperature similar to that of the air directly above. In the latter case the destabilizing effect of cloud-top radiative cooling is presumably the dominant mechanism driving the flow.

Acknowledgements

I would like to thank Hans Oerlemans for his guidance during this research and the freedom and time he gave me to tackle the problem my own way, Sjeff Zimmerman for many constructive remarks and criticisms, Huib de Swart for advise on some aspects of nonlinear stability theory and Cor Schuurmans for his contribution in making this research possible. The computer simulations were performed at the University of Utrecht.

References

- Agee, E. M., T. S. Chen and K. E. Dowell, 1973: A review of mesoscale cellular convection. *Bull. Amer. Meteor. Soc.* **54**, 1004–1012.
- Asai, T., 1970a: Three-dimensional features of thermal convection in plane Couette flow. *J. Meteor. Soc. Japan*, **48**, 18–29.
- Asai, T., 1970b: Stability of plane parallel flow with variable vertical shear and unstable stratification. *J. Meteor. Soc. Japan*, **48**, 129–139.
- Busack, B., S. Bakan and H. Luthardt, 1985: Surface conditions during mesoscale cellular convection. *Beitr. Phys. Atmosph.* **58**, 4–10.
- Christopherson, D. G., 1940: Note on the vibration of membranes. *Quart. J. Mech. Appl. Math.* **11**, 63–65.
- Clark, T. L., T. Hauf and J. P. Keutner, 1986: Convectively forced internal gravity waves: results from two-dimensional numerical experiments. *Quart. J. R. Meteor. Soc.* **112**, 899–926.
- Busse, F. H., 1967: The stability of finite amplitude convection and its relation to an extremum principle. *J. Fluid Mech.* **30**, 625–649.
- Delden, A. van, 1987: On cumulus Cloud Patterns and the theory of Shallow Convection. Phd thesis, University of Utrecht. 185 pp.
- Gollub, J. P., A. R. McCarriar and J. F. Steinman, 1982: Convective pattern evolution and secondary instabilities. *J. Fluid Mech.* **125**, 259–281.
- Haken, H., 1978: *Synergetics*. Second edition. Springer Verlag, Heidelberg. 355 pp.
- Hathaway, D. H. and R. C. J. Somerville, 1983: Three-dimensional simulation of convection in layers with tilted rotation vectors. *J. Fluid Mech.* **126**, 75–89.
- Helfand, D. M. and E. Kalnay, 1983: A model to determine open and closed cellular convection. *J. Atmos. Sci.* **40**, 631–650.
- Kondo, H., R. Kimura and S. Nishimoto, 1972: Effects of curved temperature profiles on Bénard-Rayleigh convective instability. *J. Meteor. Soc. Japan* **50**, 65–69.
- Krishnamurti, R., 1968: Finite-amplitude convection with changing mean temperature. *J. Fluid Mech.* **33**, 445–463.
- Krishnamurti, R., 1970: On the transition to turbulent convection. Part 1. The transition from two to three-dimensional flow. *J. Fluid Mech.* **42**, 295–307.
- Krishnamurti, R., 1975a: On cellular cloud patterns. Part 1. Mathematical model. *J. Atmos. Sci.* **32**, 1353–1363.
- Krishnamurti, R., 1975b: On cellular cloud patterns. Part 3. Applicability of the mathematical and laboratory models. *J. Atmos. Sci.* **32**, 1373–1383.
- Kuo, H. L. and G. Platzman, 1961: A normal mode nonlinear solution of the Rayleigh convection problem. *Beitr. Phys. Atmosph.* **33**, 137–168.
- Matveev, L. T., 1984: *Cloud Dynamics*. D. Reidel Publ. Comp., Dordrecht, 340 pp.
- Miura, Y., 1986: Aspect ratios of longitudinal rolls and convection cells observed during cold-air outbreaks. *J. Atmos. Sci.* **43**, 26–39.
- Oerlemans, J., 1986: Atmospheric convection: a re-investigation of Bjerknes' slice method. *Beitr. Phys. Atmosph.* **59**, 41–53.

- Palm, E.*, 1960: On the tendency towards hexagonal cells in steady convection. *J. Fluid Mech.* **8**, 183–192.
- Rayleigh, L.*, 1916: On convection currents in a horizontal layer of fluid, when the higher temperature is on the underside. *Phil. Mag.* **32**, 529–546.
- Schlüter, A., F. H. Busse and D. Lortz*, 1965: On the stability of steady finite-amplitude convection. *J. Fluid Mech.* **23**, 129–144.
- Scorer, R.*, 1986: Cloud Investigation by Satellite. Ellis Horwood Series Environmental Science.
- Spiegel, E. A. and G. Veronis*, 1960: On the Boussinesq approximation for a compressible fluid. *Astrophys. J.* **131**, 442–447.
- Stuart, J. T.*, 1964: On the cellular patterns in thermal convection. *J. Fluid Mech.* **18**, 481–498.
- Tennekes, H. and J. L. Lumley*, 1972: A First Course in Turbulence. MIT Press, 300 pp.
- Swart, H. E. de and J. Grasman*, 1987: Effect of stochastic perturbations on a low-order spectral model of the atmospheric circulation. *Tellus*, **39A**, 10–24.
- Veltishchev, N. F. and A. A. Zheleznin*, 1974: The effect of the unsteady nature of the mean temperature field on the structure of convective motions. *Trudy Gidromettsentra SSSR*, 1974, No. 148, p. 3.
- Veltishchev, N. F. and A. A. Zheleznin*, 1975: Numerical simulation of convection in air. *J. Fluid Mech.* **68**, 353–368.
- Walter, B. A.*, 1980: Wintertime observations of roll-clouds over the Bering Sea. *Mon. Wea. Rev.* **108**, 2024–2031.
- Weston, K. J.*, 1980: An observational study of convective cloud streets. *Tellus* **32**, 433–438.
- Young, J. A.*, 1968: Comparative properties of some time-difference schemes for linear and nonlinear oscillations. *Mon. Wea. Rev.* **96**, 357–364.

Appendix A. The Nonlinear Interaction Terms

F_z , F_w and F_θ in eqs (5.4a, b, c) are defined as follows:

$$F_z = \pi (L_{\gamma\beta\alpha} - L_{\gamma\alpha\beta}) i Z_\beta W_\alpha + M_{\gamma\alpha\beta} Z_\alpha Z_\beta - \pi^2 n_\beta^2 M_{\gamma\alpha\beta} W_\alpha W_\beta;$$

$$F_w = \pi N_{\gamma\alpha\beta} i W_\alpha W_\beta + \pi J_{\gamma\alpha\beta} i Z_\alpha Z_\beta + \pi^2 I_{\gamma\alpha\beta} Z_\beta W_\alpha;$$

$$F_\theta = \pi L_{\gamma\alpha\beta} i W_\beta \Theta_\alpha + M_{\gamma\alpha\beta} Z_\beta \Theta_\alpha.$$

Here $L_{\gamma\alpha\beta}$, $M_{\gamma\alpha\beta}$, $J_{\gamma\alpha\beta}$ and $I_{\gamma\alpha\beta}$ are coupling coefficients defined as,

$$L_{\gamma\alpha\beta} = \left\{ \frac{n_\beta (l_\alpha l_\beta a_x^2 + m_\alpha m_\beta a_y^2)}{q_\beta^2} - n_\alpha \right\} \delta_{\gamma, \alpha+\beta};$$

$$M_{\gamma\alpha\beta} = \frac{a_x a_y}{q_\beta^2} (l_\alpha m_\beta - l_\beta m_\alpha) \delta_{\gamma, \alpha+\beta};$$

$$N_{\gamma\alpha\beta} = \frac{k_\beta^2}{k_\gamma^2 q_\alpha^2 q_\beta^2} \{ 2n_\alpha (a_x^2 l_\alpha l_\beta + a_y^2 m_\alpha m_\beta)^2 + (q_\beta^2 n_\alpha - q_\alpha^2 n_\beta) (a_x^2 l_\alpha l_\beta + a_y^2 m_\alpha m_\beta) - n_\gamma q_\alpha^2 q_\beta^2 \} \delta_{\gamma, \alpha+\beta};$$

$$J_{\gamma\alpha\beta} = \frac{-2n_\beta}{k_\gamma^2} M_{\gamma\alpha\beta} M_{\gamma\beta\alpha};$$

$$I_{\gamma\alpha\beta} = \frac{1}{k_\gamma^2} (q_\beta^2 + q_\alpha^2 + n_\alpha^2 - n_\beta^2) M_{\gamma\alpha\beta} - 2 I_{\gamma\alpha\beta}^+,$$

where

$$I_{\gamma\alpha\beta}^+ = \frac{a_x a_y}{k_\gamma^2 q_\alpha^2 q_\beta^2} (q_\alpha^2 + n_\alpha^2 + n_\alpha n_\beta) \{ (a_x^2 l_\beta^2 - a_y^2 m_\beta^2) l_\alpha m_\alpha - (a_x^2 l_\alpha^2 - a_y^2 m_\alpha^2) l_\beta m_\beta \} \delta_{\gamma, \alpha+\beta}.$$

Appendix B. Symmetry Conditions

To satisfy the boundary conditions (3.9) and (3.10) the vertical velocity and temperature must have a sine-dependence in the vertical direction while the vertical vorticity must have a cosine-dependence in the vertical. For the vertical velocity this would, for example, imply that

$$W_{l,m,-n}^R = -W_{l,m,n}^R, \quad W_{l,m,-n}^I = -W_{l,m,n}^I,$$

where the superscripts, I and R denote the imaginary part and the real part of w , respectively. The fields have to be real, of course, i.e.

$$W_\gamma = W_\gamma^*,$$

or

$$W_{l,m,n}^R = W_{-l,-m,-n}^R; \quad W_{l,m,n}^I = -W_{-l,-m,-n}^I,$$

and analogous relations for Θ_γ^R , Θ_γ^I , Z_γ^R and Z_γ^I .

It can easily be deduced that these symmetry relations imply that only the equations for the evolution of the coefficients in two octants of the wave vector volume have to be integrated. The following two octants have been chosen:

$$l \geq 0, \quad n > 0.$$

All coefficients θ and w with $n=0$ are zero. This follows from the symmetry relations above. As to the coefficients of ζ with $n=0$, these may possibly be different from zero, implying that a vertical mean flow can be generated. The possibility of this effect will, however be ignored. Furthermore, the possibility of horizontal mean flow generation, known to occur in fluid layers subject to tilted rotation (Hathaway and Sommerville, 1983), will also be ignored.

The equations are integrated in time using Young's (1968) method 'A' with a time step, $\Delta t = 0.0005$. On the CYBER-180-855 the program costs 5.8 to 6.1 seconds central processor unit time per timestep. This is very expensive compared to when finite difference methods are used (see e.g. Orszag, 1971). It is the price that is paid for the high accuracy of this so-called

"interaction coefficient spectral method". The accuracy of the model of course depends on Δt . This has been tested by checking how well the total kinetic energy is conserved by the advection terms. At $\Delta t = 0.0005$ the kinetic energy was reasonably well conserved over one time unit, which is a relatively long time period in the atmospheric context (see section 8) (van Delden, 1987).

Appendix C. The Low-Order Model of Poloidal Convection

In the low-order model of poloidal convection the horizontal dependence of both θ and w is represented by cosine series. For the vertical velocity this implies that

$$W_{l,m,n}^R = W_{l,-m,n}^R = W_{-l,m,n}^R. \quad (C1)$$

Together with the symmetry relations described in appendix B, this in turn implies that $W_{l,m,n}^R = 0$. The same reasoning applies to the temperature. Due to these extra symmetry relations only equations for the imaginary parts of the coefficients corresponding to one octant of wave-vector space are needed. The octant $l \geq 0, m \geq 0$ and $n \geq 0$ is chosen.

All possible low-order model interactions are listed in Table 4. It is then straightforward to derive the model equations using the definition of the coupling coefficients given in appendix A. If it is assumed that $a_x^2 = 3a_y^2 = 3a^2$, these equations become

$$\begin{aligned} \frac{d\Theta_{111}}{dt} = & -\frac{3}{2}\pi W_{111}\Theta_{022} - \frac{3}{2}\pi W_{021}\Theta_{112} + \pi\Theta_{001}W_{112} - \\ & - 2\pi\Theta_{002}W_{111} - 3\pi\Theta_{003}W_{112} + Ra W_{111} - \\ & - \pi^2(4a^2 + 1)\Theta_{111}; \end{aligned}$$

$$\begin{aligned} \frac{d\Theta_{112}}{dt} = & \frac{3}{2}\pi W_{021}\Theta_{111} + \frac{3}{2}\pi W_{111}\Theta_{021} + \pi\Theta_{001}W_{111} - \\ & - 3\pi\Theta_{003}W_{111} - 4\pi\Theta_{004}W_{112} + Ra W_{112} - \\ & - \pi^2(4a^2 + 4)\Theta_{112}; \end{aligned}$$

$$\begin{aligned} \frac{d\Theta_{021}}{dt} = & -3\pi W_{111}\Theta_{112} + \pi\Theta_{001}W_{022} - 2\pi\Theta_{002}W_{021} - \\ & - 3\pi\Theta_{003}W_{022} + Ra W_{021} - \pi^2(4a^2 + 1)\Theta_{021}; \end{aligned}$$

$$\begin{aligned} \frac{d\Theta_{022}}{dt} = & 3\pi W_{111}\Theta_{111} + \pi\Theta_{001}W_{021} - 3\pi\Theta_{003}W_{021} - \\ & - 4\pi\Theta_{004}W_{022} + Ra W_{022} - \pi^2(4a^2 + 4)\Theta_{022}; \end{aligned}$$

$$\begin{aligned} \frac{d\Theta_{001}}{dt} = & -4\pi W_{111}\Theta_{112} - 4\pi W_{112}\Theta_{111} - 2\pi W_{021}\Theta_{022} - \\ & - 2\pi W_{022}\Theta_{021} - \pi^2(\Theta_{001} - \bar{\Theta}_{001}); \end{aligned}$$

$$\begin{aligned} \frac{d\Theta_{002}}{dt} = & 8\pi W_{111}\Theta_{111} + 4\pi W_{021}\Theta_{021} - \\ & - 4\pi^2(\Theta_{002} - \bar{\Theta}_{002}); \end{aligned}$$

$$\begin{aligned} \frac{d\Theta_{003}}{dt} = & 12\pi W_{111}\Theta_{112} + 12\pi W_{112}\Theta_{111} + \\ & + 6\pi W_{021}\Theta_{022} + 6\pi W_{022}\Theta_{021} - \\ & - 9\pi^2(\Theta_{003} - \bar{\Theta}_{003}); \end{aligned}$$

$$\begin{aligned} \frac{d\Theta_{004}}{dt} = & 16\pi W_{112}\Theta_{112} + 8\pi W_{022}\Theta_{022} - \\ & - 16\pi^2(\Theta_{004} - \bar{\Theta}_{004}); \end{aligned}$$

Table 4 Non-zero interactions taken inside the truncation in the low-order model. The interaction of the wave-vectors α and β , contributes to the wave-vector, γ . The interactions are subdivided into classes which are defined in appendix E.

Class 1 interactions			Class 2 interactions			Class 3 interactions		
γ	α	β	γ	α	β	γ	α	β
(0, 0, 1)	(1, 1, -1)	(-1, -1, 2)	(1, 1, 1)	(1, 1, 2)	(0, 0, -1)	(0, 2, 1)	(1, 1, -1)	(-1, 1, 2)
(0, 0, 1)	(-1, -1, -1)	(1, 1, 2)	(1, 1, 1)	(1, 1, -1)	(0, 0, 2)	(0, 2, 1)	(-1, 1, -1)	(1, 1, 2)
(0, 0, 1)	(-1, 1, -1)	(1, -1, 2)	(1, 1, 1)	(1, 1, -2)	(0, 0, 3)	(1, 1, 1)	(1, -1, -1)	(0, 2, 2)
(0, 0, 1)	(1, -1, -1)	(-1, 1, 2)	(0, 2, 1)	(0, 2, 2)	(0, 0, -1)	(1, 1, 2)	(1, -1, 1)	(0, 2, 1)
(0, 0, 2)	(1, 1, 1)	(-1, -1, 1)	(0, 2, 1)	(0, 2, -1)	(0, 0, 2)	(0, 2, 2)	(-1, 1, 1)	(1, 1, 1)
(0, 0, 2)	(-1, 1, 1)	(1, -1, 1)	(0, 2, 1)	(0, 2, -2)	(0, 0, 3)	(1, 1, 1)	(1, -1, 2)	(0, 2, -1)
(0, 0, 3)	(1, 1, 1)	(-1, -1, 2)	(1, 1, 2)	(1, 1, 1)	(0, 0, 1)			
(0, 0, 3)	(-1, -1, 1)	(1, 1, 2)	(1, 1, 2)	(1, 1, -1)	(0, 0, 3)			
(0, 0, 3)	(-1, 1, 1)	(1, -1, 2)	(1, 1, 2)	(1, 1, -2)	(0, 0, 4)			
(0, 0, 3)	(1, -1, 1)	(-1, 1, 2)	(0, 2, 2)	(0, 2, 1)	(0, 0, 1)			
(0, 0, 4)	(1, 1, 2)	(-1, -1, 2)	(0, 2, 2)	(0, 2, -1)	(0, 0, 3)			
(0, 0, 4)	(-1, 1, 2)	(1, -1, 2)	(0, 2, 2)	(0, 2, -2)	(0, 0, 4)			
(0, 0, 1)	(0, 2, -1)	(0, -2, 2)						
(0, 0, 1)	(0, -2, -1)	(0, 2, 2)						
(0, 0, 2)	(0, 2, 1)	(0, -2, 1)						
(0, 0, 3)	(0, 2, 1)	(0, -2, 2)						
(0, 0, 3)	(0, -2, 1)	(0, 2, 2)						
(0, 0, 4)	(0, 2, 2)	(0, -2, 2)						

$$\begin{aligned}
\frac{dW_{111}}{dt} &= -\frac{3}{2}\pi W_{022}W_{111} - \frac{3}{2}\pi W_{021}W_{112} + \\
&\quad + \frac{4a^2\text{Pr}}{4a^2+1}\Theta_{111} - \pi^2\text{Pr}(4a^2+1)W_{111}; \\
\frac{dW_{112}}{dt} &= 3\pi\frac{4a^2+1}{4a^2+4}W_{111}W_{021} + \frac{4a^2\text{Pr}}{4a^2+4}\Theta_{112} - \\
&\quad - \pi^2\text{Pr}(4a^2+4)W_{112}; \\
\frac{dW_{021}}{dt} &= -3\pi W_{112}W_{111} + \frac{4a^2\text{Pr}}{4a^2+1}\Theta_{021} - \\
&\quad - \pi^2\text{Pr}(4a^2+1)W_{021}; \\
\frac{dW_{022}}{dt} &= 3\pi\frac{4a^2+1}{4a^2+4}W_{111}^2 + \frac{4a^2\text{Pr}}{4a^2+4}\Theta_{022} - \\
&\quad - \pi^2\text{Pr}(4a^2+4)W_{022},
\end{aligned}$$

where the commas in the subscripts and the superscripts have been omitted to save space. It can be verified (van Delden, 1987) that potential energy and kinetic energy are conserved by the nonlinear terms. The hexagonal solution of Christopherson (1940) (4.1) is equivalent to having,

$$\begin{aligned}
\Theta_{111} &= \Theta_{021}; \quad \Theta_{112} = \Theta_{022}; \\
W_{111} &= W_{021}; \quad W_{112} = W_{022}.
\end{aligned} \tag{C2}$$

When substituting these equations into the low-order model equations above, it is found that,

$$\begin{aligned}
\frac{d\Theta_{111}}{dt} &= \frac{d\Theta_{021}}{dt}; \quad \frac{d\Theta_{112}}{dt} = \frac{d\Theta_{022}}{dt}; \\
\frac{dW_{111}}{dt} &= \frac{dW_{021}}{dt}; \quad \frac{dW_{112}}{dt} = \frac{dW_{022}}{dt},
\end{aligned}$$

which implies that (C2) is a solution of the model. Unfortunately, it is impossible to obtain an analytical expression for the coefficients as a function of the parameters, a , Ra and Pr , corresponding to the hexagonal solution.

In this model the flow has the freedom to choose between a hexagon with upward flow (a "up-hexagon") or downward flow (a "down-hexagon") in the centre, or a roll, both with a nondimensional wavelength (aspect ratio) equal to a^{-1} . Other less well defined solutions are also possible.

The solution of the low-order model is used as initial condition for the higher order model in which the constraint (C1) is dropped and the flow is allowed to become toroidal. The higher-order model consists of 1096 coupled nonlinear differential equations.

Appendix D. Definition of Kinetic Energy

The total kinetic energy, K , is defined as,

$$K = \frac{1}{2} \int \vec{v} \cdot \vec{v} \, d\sigma.$$

Transforming this equation is a matter of substituting the expansion (4.2) and using (5.1), (5.2a,b) and the symmetry relations defined in appendix B to obtain,

$$K = K_T + K_P,$$

where K_T and K_P are, respectively, the toroidal and poloidal parts of the kinetic energy, defined as,

$$K_T = \frac{1}{2} \sum_{\gamma} \frac{1}{\pi^2 q_{\gamma}^2} Z_{\gamma} Z_{\gamma}^*;$$

$$K_P = \frac{1}{2} \sum_{\gamma} \frac{k_{\gamma}^2}{\pi^2 q_{\gamma}^2} W_{\gamma} W_{\gamma}^*.$$

Appendix E. Some Properties of Nonlinear Interactions

The wave vectors α and β interact to contribute to wave vector γ only if the selection rule,

$$l_{\alpha} + l_{\beta} = l_{\gamma}; \quad m_{\alpha} + m_{\beta} = m_{\gamma}; \quad n_{\alpha} + n_{\beta} = n_{\gamma},$$

is satisfied. The interaction may be divided into three classes:

- class 1: wave-wave interactions contributing to the mean state;
- class 2: wave-mean interactions contributing to the waves;
- class 3: wave-wave interactions contributing to the waves.

The mean state is given by all modes with $l_{\gamma} = m_{\gamma} = 0$ (i.e. the horizontal mean). For the waves we have $l_{\gamma} \neq 0$ and/or $m_{\gamma} \neq 0$. Class 1 and 2 interactions are usually called the "mean field interactions".

For class 1 interactions one has $l_{\alpha} = -l_{\beta}$ and $m_{\alpha} = -m_{\beta}$. This has some simplifying consequences for the coupling coefficients defined in appendix A, i.e.:

$$L_{\gamma\alpha\beta} = -n_{\gamma} \delta_{\gamma, \alpha+\beta},$$

$$M_{\gamma\alpha\beta} = 0,$$

$$N_{\gamma\alpha\beta} = J_{\gamma\alpha\beta} = I_{\gamma\alpha\beta} = I_{\gamma\alpha\beta}^+ = 0.$$

The second relation implies that *the toroidal part of the motion field has no influence on the horizontal mean stratification.*

For class two interactions (the "feedback" of class 1), one of the interacting wave vectors is the mean state.

Therefore, either $l_\alpha = m_\alpha = 0$ or $l_\beta = m_\beta = 0$. This implies that,

$$L_{\gamma\alpha\beta} = -n_\alpha \delta_{\gamma, \alpha+\beta},$$

$$M_{\gamma\alpha\beta} = 0,$$

$$N_{\gamma\alpha\beta} \equiv J_{\gamma\alpha\beta} = I_{\gamma\alpha\beta} = I_{\gamma\alpha\beta}^+ = 0$$

for class 2 interactions.

For class 3 interactions less sweeping general statement can be made. Nevertheless, closer examination of the interaction coefficients reveals that for interacting wave vectors, α and β , with $q_\alpha = q_\beta$ and $n_\alpha = n_\beta$, all class 3 interactions in the vorticity (Z) equation vanish because

$$M_{\gamma\alpha\beta} = -M_{\gamma\beta\alpha} \quad \text{and} \quad L_{\gamma\alpha\beta} = L_{\gamma\beta\alpha}.$$

This result (derived in a different way) can also be found in the analysis of Schlüter et al. (1965). In other words, if the flow pattern consists of Fourier modes of equal total horizontal and vertical wave numbers, such as a hexagon or square, no kinetic energy will flow to the toroidal part of the flow field. However, the nonlinear terms in the equation for W_γ (5.4b) do not vanish in this case. Higher harmonics, which do not satisfy the above equalities, may be excited. Nevertheless, since these higher harmonics will have much smaller amplitudes, especially those with $n > 1$, which at $Ra < 10^4$ are all damped, the toroidal modes will necessarily also have small amplitudes. These statements suggest that, if convection is dominated by modes with equal total horizontal wave numbers (q) and equal vertical wave numbers (n), and if there is no rotation, little energy will flow to the toroidal part of the flow-field through nonlinear interactions.